

# IPM Synchronous Motor for Traction Applications: Performance Analysis Considering Airgap Variation

**Abstract.** Recently, Inner Permanent Magnet (IPM) Synchronous Motors are known as a good candidate for hybrid electric vehicle traction drive application due to their unique merits like little volume, light weight, high efficiency and power factor and high reliability. However, behavior of this motors is quite depending on airgap length. This paper discusses the effect of airgap variation on d-q equivalent circuit model, also presents a novel structure of IPM synchronous motor for traction application with three layers of fragmental buried rotor magnets in order to achieve less torque ripple, iron losses and cogging torque, higher power factor and improving the electromagnetic torque per ampere and simulation of this motor. Thus, in order to extract the output values of motor and sensitivity analysis on hysteresis loop characteristics using 3D-Finite element model, then shows the back EMF, power factor, cogging torque, flux density, torque per ampere diagram of the IPM synchronous motor with variation of hard magnetic material hysteresis loop characteristics in rotor structure. This study can help designers in design approach of such motors.

**Streszczenie.** W artykule przedstawiono zagadnienie wpływu wahań szerokości szczeliny powietrznej w maszynie synchronicznej z magnesami trwałymi (PMSM) na jej model matematyczny we współrzędnych d-q oraz nową strukturę PMSM z trzema częściowo zakrzębanymi warstwami magnesów wirnika na potrzeby trakcji. Proponowana budowa wpływa na redukcję m.in. wahań momentu maszyny, strat w żelazie, momentu zaczepowego, wzrost współczynnika mocy. Analizę przeprowadzono z wykorzystaniem metody elementów skończonych w 3-D. (**Silnik synchroniczny z magnesami trwałymi w trakcji elektrycznej – wpływ wahań szerokości szczeliny powietrznej na pracę maszyny**).

**Keywords:** Airgap; IPM synchronous motor; Design; 3D-FEM Model; Dynamic model; Traction.

**Słowa kluczowe:** szczelina powietrzna, PMSM, model 3-D FEM, model dynamiczny, trakcja.

## Introduction

IPM synchronous machine has many advantages such as high power density, efficiency and wide speed operation, these advantages make it particularly suitable for automotive, traction applications where space, weight and geometry dimensions are very important [1]-[9].

The main features of this motors for hybrid electric vehicle traction drive application are simple construction with conventional three phase stator windings with low current density, rotor with inner fragmental permanent magnet (PM) [1]-[4], but this paper presents a novel structure of rotor to achieve low torque ripple, iron losses and cogging torque. It is known that the efficiency, linkage flux, back EMF, power factor and torque behavior of these motors could be easily affected by airgap length [7]-[11]. Regarding this issue, effect of airgap length on d-q equivalent circuit model is perused and effect of airgap variation on back EMF, power factor, cogging torque, flux density, torque per ampere diagram of the IPM synchronous motor is investigated separately. Meanwhile, the finite element method (FEM) is implemented for accurate simulation, this 3D-finite element model has high level of accuracy and gives a better insight of motor performance. All in all, the objective of this paper is to derive the performance characteristics of IPM synchronous motors and to perform sensitivity analysis of such motors at synchronous speed based on 3D-FEM.

Also, this model can be used in the design approach and precise analysis of inner permanent magnet synchronous motors for hybrid electric vehicle traction drive application.

## Structure and Winding Configuration

As shown in Fig. 1(a), a 80-kW, 8pole, 48 slots and 6 slots per pole for possible hybrid electric vehicle application (in order to achieve harmonic reduction [12]) IPM synchronous machine has been designed with three layers of fragmental buried rotor magnet (in order to achieve MTPA), but all of these layers have a trapezoid structure as shown in Fig. 1(b) for reduce hot spots (zones that have maximum flux density).

In this machine a kind of permanent magnet material in rotor structure has been used which has suitable reversible

temperature coefficients as it can be seen in Table 1 [13]. Also, laminations of permendur-24 for constructing the stator and rotor cores, and a kind of stainless steel with very low relative permeability in shaft structure has been used. Soft magnetic material (permendur-24) characteristics are given in table 2 [14].

The stator slots are embedded with three layer fractional-slot (5/6) windings with 18 conductors per stator slot and each phase contains eight turns of windings (to achieve harmonic reduction), current density in windings is 4.2 A/mm<sup>2</sup> and radius of each naked wire is 2.936 mm by using insulators F-class. The winding diagram and terminal connection mode of the 8-pole stator winding has been shown in Fig. 2. Model analyses have been performed at one half pole by 3D-finite element method (FEM).

## Fem model

As mentioned before, a 3D-finite element model which gives a better insight of motor performance is implemented in order to simulate of proposed motor.

In order to have high level of accuracy the automatic mesh diagram is not used and a mesh diagram is designed manually and node congestion is higher around the air gap. The total number of nodes is about 190000 which lead to high accuracy. Meanwhile, for boundary conditions, the homogenous Dirichlet condition has been adopted on the infinite box that encompasses the motor.

This simulation has been based on circuit coupled model using the phase voltage as input. Fig. 3 shows the circuit coupled model which has been used in this study, for each phase eight coil winding is considered, four coils of them send the current in motor and four coils return current from midpoint of winding in star connection. Coil winding connection in each phase is exactly the same that is illustrated in Fig. 2(b).

## Permanent magnet material volume

Figure 4 helps to exploit the hysteresis loop, in order to choose an accurate volume of hard magnetic material, an iteration method is used that is illustrated with a flow chart in Figure 5, in the first iteration, PM volume is obtained by using [15]:

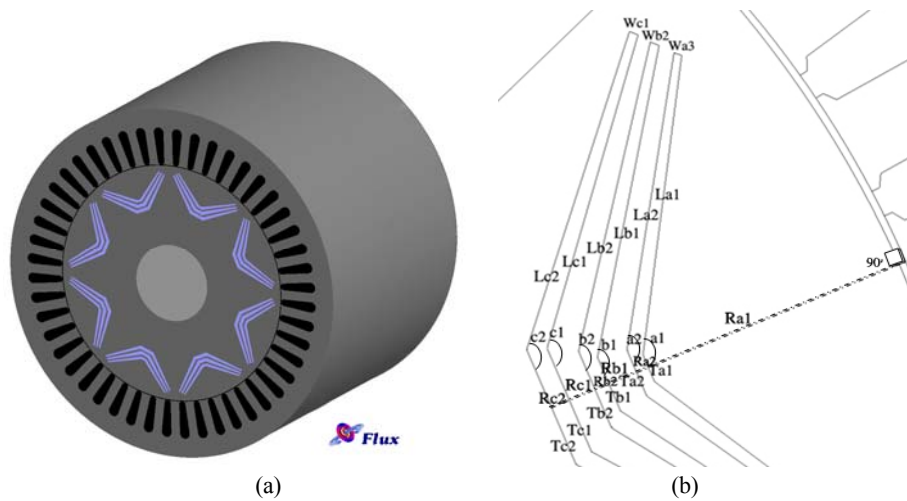


Fig. 1. 8-pole, 48 slot inner permanent magnet synchronous motor structure for traction application with three layers of fragmental buried rotor magnets, (b) Novel structure of rotor.

Table 1. Permanent magnet characteristics

Parameters	$B_r$ (T)	$H_c$ (KA/m)	$\mu_r$	$T_{max}$ ( $^{\circ}$ C)	$T_{ciure}$ ( $^{\circ}$ C)	$T_c$ of $B_r$	$T_c$ of $H_c$
Sintered $Sm_2Co_{17}$	1	820	1.05	300	750	-0.04	-0.3

Table 2. Soft magnetic material characteristics

Parameters	Saturation flux density (T)	Remanence (T)	Initial permeability	maximum permeability
Permendur-24	2.34	1.5	250	2000

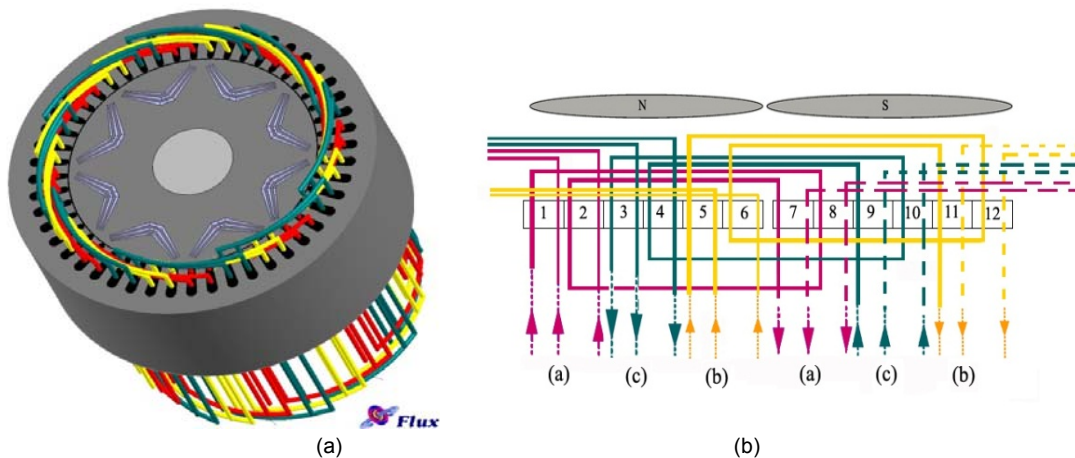


Fig. 2. (a) Winding diagram- (b) a pair pole stator terminal connection of 8-pole inner PMSM with three layer distributed windings

$$(1) \quad V_m = \frac{c_v \cdot P_{out}}{F \cdot B_r \cdot H_c}$$

$C_v$  is a coefficient that depending on the PM design in rotor structure and approximated between 0.54 to 3.1. From the FEA, the back EMF in each phase can be obtained and its amplitude value is checked with amplitude value of input voltage in each phase and this procedure continues until the convergence criterion is satisfied. As it can be observed from the simulation results, this procedure is so effective for choosing type and volume of PM which has close agreement with real motor tests.

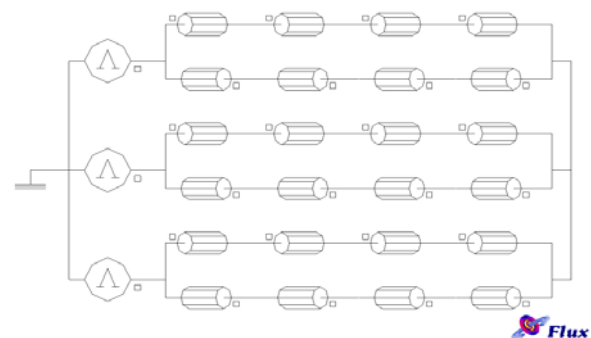


Fig. 3. Circuit coupled model used in simulation



Fig. 4. Sm<sub>2</sub>Co<sub>17</sub> hysteresis loop

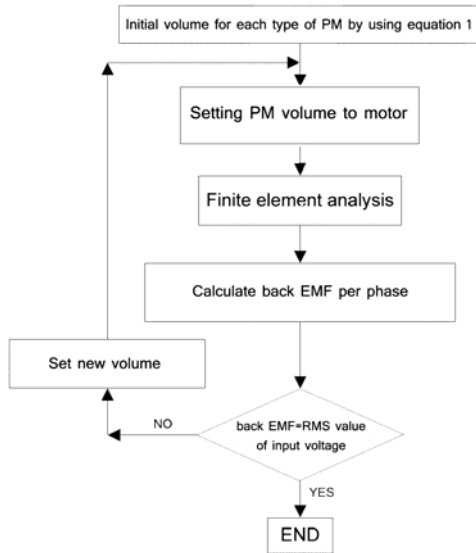


Fig. 5. Flowchart for accurate volume of PM selection

### Effect of airgap length on electrical model

Effect of airgap length on electrical model and output electromagnetic torque of IPM synchronous motor, clearly is obtained by using equations 2 to 14, average air gap flux density as follows [9],[10]:

$$(2) \quad B_g = \frac{C_\Phi}{1 + \beta(1 + 2\eta + 4\lambda)} B_r$$

Where  $C_\Phi = Am / Ag$  is the flux concentration factor.

The values of parameters in equation 2 are given by:

$$(3) \quad \beta = \frac{\mu_r k_c g C_\Phi}{w_m}$$

$$(4) \quad \eta = \frac{w_1(h_1 + h_2)}{4d \mu_r l_m}$$

$$(5) \quad \lambda = \frac{1 + \frac{1}{\beta} + 2\eta}{2 \frac{A_m B_r}{A_m B_s} - 4}$$

where KC is the Carter coefficient,  $A_m = t \cdot l$  represents the cross sectional area of the iron bridge above the nonmagnetic barriers with  $t$  and  $l$  being the bridge width and motor stack length, respectively. Also  $h_1$  and  $h_2$  represent the inner and the outer flux barrier heights respectively, while  $B_s$  is a limit of the leakage flux density in the bridge due to saturation.

The maximum value of first harmonic of PM flux linkage is obtained as [10]:

$$(6) \quad \Psi_M = \frac{4Dl}{\pi} \left( \frac{K_{w1} N_{ph}}{p} \right) B_g \sin\left(\frac{\alpha\pi}{2}\right)$$

where  $K_{w1}$  is the winding factor. The inductances of d-axis and q-axis are given by [7],[9]:

$$(7) \quad L_d = \frac{3\mu_0 D l}{g} \left( \frac{K_{w1} N_{ph}}{p} \right)^2 \frac{\pi}{8} K_d$$

$$(8) \quad L_q = \frac{3\mu_0 D l}{g} \left( \frac{K_{w1} N_{ph}}{p} \right)^2 \frac{\pi}{8} K_q$$

where  $K_d$  and  $K_q$  are defined as:

$$(9) \quad K_d = \left( \alpha - \frac{\sin(\alpha\pi)}{\pi} \right) + \frac{g}{g_e} \left( 1 - \alpha + \frac{\sin(\alpha\pi)}{\pi} \right)$$

$$(10) \quad K_q = \left( \alpha + \frac{\sin(\alpha\pi)}{\pi} \right) + \frac{g}{g_e} \left( 1 - \alpha - \frac{\sin(\alpha\pi)}{\pi} \right)$$

and  $g_e$  denotes an effective air gap and is given by:

$$(11) \quad g_e = K_c g$$

A conventional d-q electrical model of the machine in a synchronously rotating reference frame can be used in design optimization and evaluation. In this model the flux distribution in the air gap is assumed to be sinusoidal and the iron loss and magnetic saturation are not considered [7],[9].

The motor vector diagram is shown in Fig. 6, voltage Equations are expressed as follows [9]:

$$(12) \quad V \sin(\delta) = i_d R_1 + \omega i_q L_q$$

$$(13) \quad V \cos(\delta) = i_q R_1 - \omega i_d L_d + E_f$$

The motor torque is then obtained as:

$$(14) \quad T = \frac{3p}{2} (\Psi_M + (L_d - L_q) i_d) i_q$$

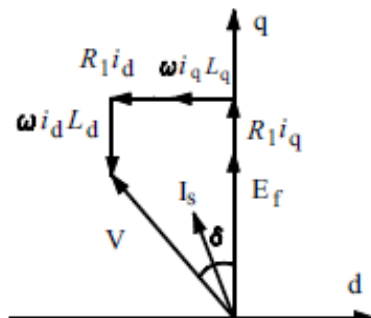


Fig. 6. IPM synchronous motor vector diagram

### Simulation Results and Discussion

Based on the above respects, finite element simulation for the IPM synchronous motor has been done, the simulation research has been made for a 8 poles prototype IPM synchronous motor, the parameters of the prototype IPM synchronous motor and the output quantities of motor for 1.6 mm air gap are given in Table 3.

It must be noted that one half pole is analyzed because of the magnetic symmetry of the motor, as seen in Figure 7 nodes congestion becomes higher near the air gap in order to accurate simulation, based on FEM model the simulation of motor is done and output characteristics are extracted.

Figure 8 shows the distribution of flux, as discusses the section, in this study flux lines are circumferentially the center of pole and distances between PM and air gap. Figure 9 shows the isovalues diagram of flux density at rated power, it can be seen that maximum flux density is

less than saturation flux density of permendur-24 and close to the saturation point of this material, air gap flux density over a predefined path (for 4 pole) is shown in Figure 10 at rated power.

Back EMF for one phase is shown in Figure 11, it can be seen that amplitude value of back EMF per phase is equal to amplitude value of input voltage per phase.

Table 4. Optimized IPM synchronous machine performance at rated speed.

Characteristic	Output
Power factor (%)	97
Total Iron loss (w)	3090
Cogging torque (N.m)	18.1
PM volume (cm3)	7488
Total copper loss (w)	2036
Electromagnetic torque at I=53.2 Ampere (N.m)	994.1

Table 4 verifies suitable performance of this IPM synchronous machine at rated speed. As it can be seen

Table 3. Motor features

Quantity	Value	Quantity	Value
Rated voltage (V)	900	Outer diameter of stator (mm)	734
Rated power (Kw)	80	Inner diameter of stator (mm)	498
Frequency (Hz)	50	Stator stack height (mm)	560
Speed (rpm)	750	Type of Winding	Double layer concentric with consequent poles
Phase connection	Y	Number of conductors per slot	20
Pole pairs	4	Core material (stator and rotor)	Permendur-24
Number of stator slots	48	Air gap length (mm)	1.6

from this table, with this novel structure (trapezoid form fragmental buried magnet), cogging torque is less than 2% of rated torque, but cogging torque in conventional IPM synchronous machines is about 5% of rated torque. but cogging torque in conventional IPM synchronous machines is about 5% of rated torque.

Now by changing the airgap length from 1.5 mm to 4 mm, the variation of IPM synchronous motor performance and output quantities are investigated.

Motor torque variation versus airgap length variation is shown in Figure 12, by increasing the airgap length the saliency ratio ( $\xi$ ) will be decreased ( $\xi$  is defined as the ratio between the q-axis inductance ( $L_q$ ) over the d-axis inductance ( $L_d$ )) [7]:

$$(15) \quad \xi = \frac{g_e + \frac{2l_m}{3\mu_r}}{g_e + \frac{l_m}{3\mu_r}}$$

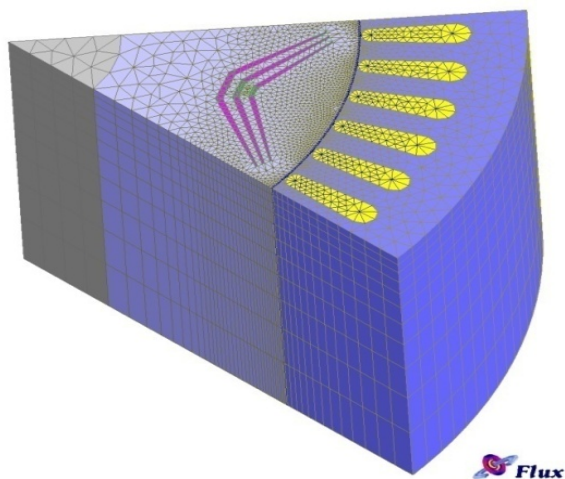


Fig. 7. Mesh diagram of simulated machine

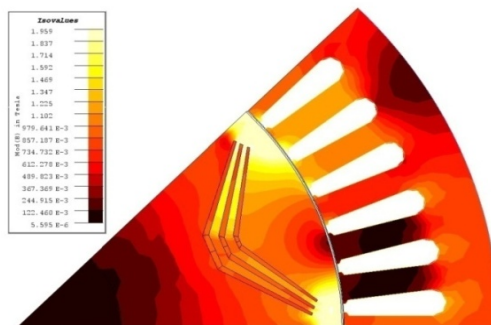


Fig. 9. Isovalues diagram of flux density at rated power

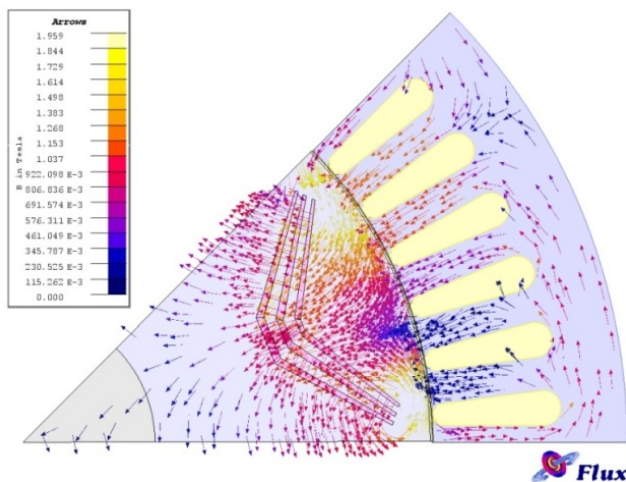
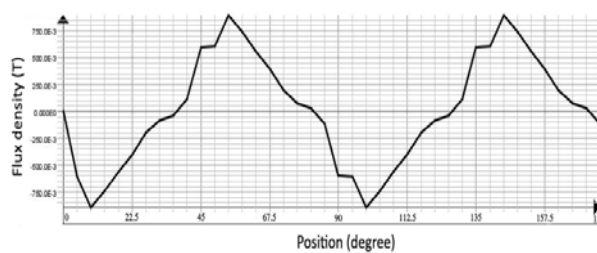
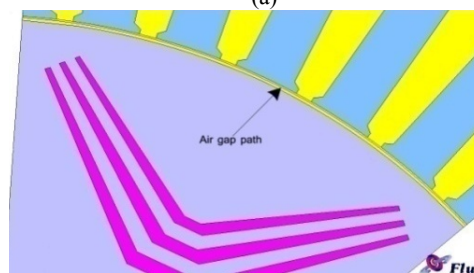


Fig. 8. Distribution of flux at rated current



(a)



(b)

Fig.10. (a) Air gap flux density diagram over the path (4 pole) (b) Air gap path belong a pole.

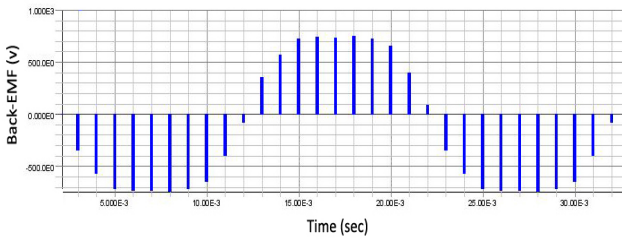


Fig. 11. Back EMF for phase (a)

By decreasing the saliency ratio, motor torque will be decreased and it can be obtained by:

$$(16) \quad T = \frac{3P}{2} (\Psi_M + L_d (1 - \xi) i_d) i_q$$

Figure 13 demonstrates the variations of cogging torque versus airgap length variation, from this Figures, it can be seen with this structure (trapezoid fragmental buried magnet), cogging torque for all prototypes is less than 1.8% of rated torque and by increasing the airgap length, cogging torque will be decreased.

Cogging torque is the consequence of interaction (magnetic attraction) between rotor-mounted permanent magnets field and the stator teeth, which produces reluctant variations on the rotor position; it is stator current independent. It manifests itself by rotor tendency to align with the stator in a number of stable positions (where the permeance of the permanent magnets' magnetic circuit is maximized), even when machine is unexcited, resulting in a pulsating torque, which does not contribute to the net effective torque. Optimizing cogging torque to a low value can be obtain a low torque ripple and harmonic reduction [13],[16]-[18].

Figure 14 demonstrates the variations of power factor versus airgap length variation, and it can be seen by increasing the airgap length, saliency ratio and after that power factor will be decreased.

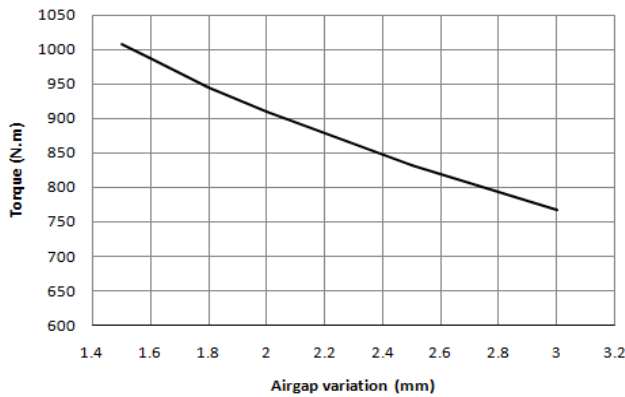


Fig. 12. Torque variation versus airgap length variation

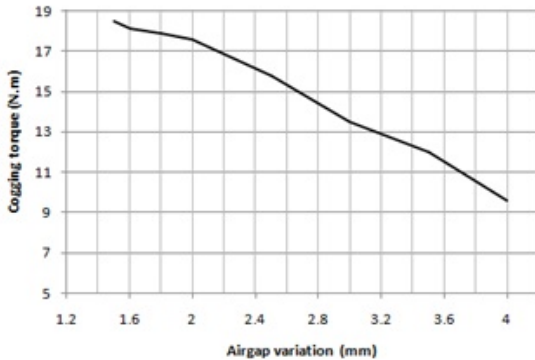


Fig 13. Cogging torque variation versus airgap length variation

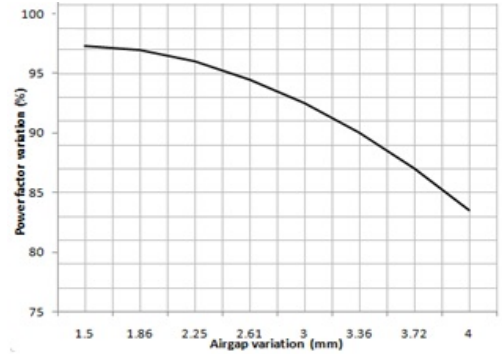


Fig. 14. Power factor variation versus variation of airgap length

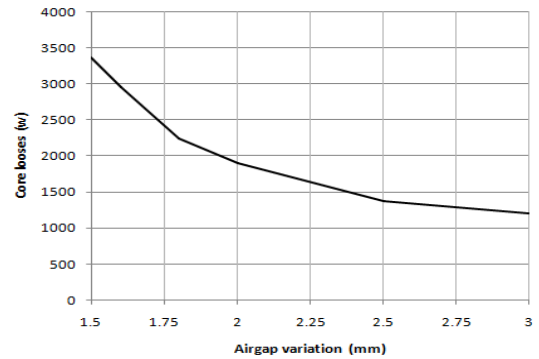


Fig. 15. Core losses variation versus variation of airgap length

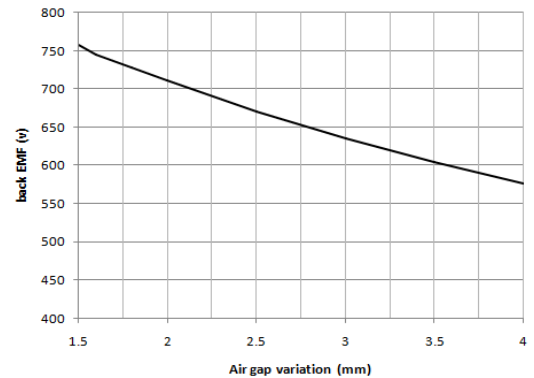


Fig. 16. Back EMF variation versus variation of airgap length

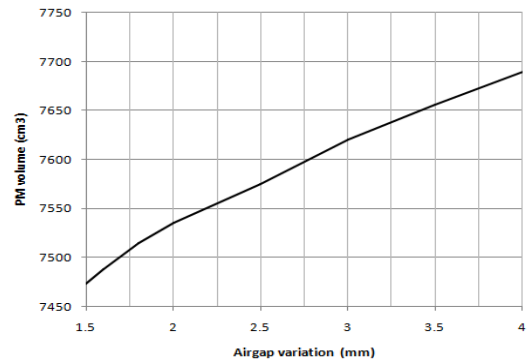


Fig. 17. Needed PM volume versus variation of airgap length

Figure 15 demonstrates the variations of core losses versus airgap length variation, it can be seen by increasing the airgap length, flux density in rotor and stator core will be decreased and thereupon hysteresis and eddy current losses of motor will be decreased. Obviously it's clear that increasing the airgap length makes decreasing of the back EMF, circumstances of this variation is shown in Figure 16. Finally, needed volume of PM for compensate of this back EMF decreasing, that obtained by flowchart Figure 5, is shown in Figure 17.

## Conclusions

This paper presents a novel structure of rotor to achieve decreasing the torque ripple, iron losses and cogging torque for IPM synchronous machines. In this structure, three layers of PM have been used and each layer has a fragmental trapezoid structure as shown before, with this structure, hot spots (zones that have maximum flux density) will be reduced. Furthermore, in order to achieve the optimal dimension of PM, an iteration method has been used that illustrated with a flowchart. The simulation has been done based on optimal dimensions and a 3D-finite element model implemented in order to simulate the IPM synchronous machine and presents output quantity of motor by having 1.6 mm airgap length.

Furthermore, this paper presents torque, cogging torque, power factor, core losses, back EMF and needed PM volume considering variation of airgap length from 1.5 mm to 4 mm. Simulation results verify the authenticity of this iteration method and advantages of this novel structure.

## Nomenclature

F	Frequency (Hz)
$V_m$	Volume of PM ( $m^3$ )
$B_r$	Remanent magnetization (Tesla)
$H_c$	Coercive force (kA/m)
$\mu_r$	Relative permeability of PM
$\mu_0$	Permeability of vacuum
T	Temperature ( $^{\circ}C$ )
A	Area ( $m^2$ )
R	Resistance ( $\Omega$ )
$P_{out}$	Motor output power (w)
$l_m$	Axial length of PM (m)
l	Axial length of motor (m)
$w_m$	width of PM (m)
g	Airgap length (mm)
p	Number of pole pairs
$N_{ph}$	Winding turns per phase
$A_g$	Pole cross section of air gap ( $m^2$ )
$A_m$	Pole cross section of PM ( $m^2$ )
$\alpha$	Pole arc to pole pitch ratio
D	Inner diameter of the stator
$\omega$	Angular Velocity (rad/s)
L	Inductance (H)
i	Stator current (A)
<i>Subscripts and Superscripts</i>	
d,q	Direct, quadrature axis component
r,s	Rotor, stator

## REFERENCES

- [1] Y. Honda, T. Nakamura, T. Higaki, Y. Takeda, " Motor Design Considerations and Test Results of an Interior Permanent Magnet Synchronous Motor for Electric Vehicles ", 32nd IAS, New Orleans, LA, Oct 5-9, 1997.
- [2] R. H. Staunton, S. C. Nelson, P. J. Otaduy, J. W. M. Keever, J. M. Bailey, S. Das, R. L. Smith, " PM Motor Parametric Design Analyses for a Hybrid Electric Vehicle Traction Drive Application ", National Lab Oak Ridge, U.S DEP of Energy, Sep 2004.
- [3] Y. Fujishima, S. Wakao, M. Kondo, and N. Terauchi, " An Optimal Design of Interior Permanent Magnet Synchronous Motor for the Next Generation Commuter Train ", IEEE Trans. on Applied Super conductivity, vol. 14, no. 2, Jun 2004.
- [4] A. Wang, H. Li and C.T. Liu, " On the Material and Temperature Impacts of Interior Permanent Magnet Machine for Electric Vehicle Applications ", IEEE. Trans. on Magnetics, vol. 44, no. 11, Nov 2008.
- [5] J. E. Gould, " Permanent Magnet Applications ", IEEE. Trans. on Magnetics, vol. Mag-5, no. 4, Dec 1969.
- [6] Wen L. Soong, N. Ertugrul, " Field-Weakening Performance of Interior Permanent-Magnet Motors ", IEEE Trans. on industry applications, vol. 38, no. 5, Sep/Oct 2002.
- [7] Y. K. Chin, " A Permanent-Magnet Synchronous Motor for an Electric Vehicle Design Analysis ", Ph.D. dissertation, Dept. of . Electrical Eng. KTH Univ., Stockholm, Jul 2004.
- [8] Y. K. Chin, J. Soulard, " Design Study of a Traction Motor for Electric Vehicles ", conference on Electrical Machines and System, ICEMS 2005.
- [9] A. H. Isfahani, S. Sadeghi, "Design of a Permanent Magnet Synchronous Machine for the Hybrid Electric Vehicle," World Academy of Science, Engineering and Technology, Vol. 2, No. 1, pp. 566-570, 2008.
- [10] C.C. Hwang, S.M. Chang, C.T. Pan, T.Y. Chang, "Estimation of Parameters of Interior Permanent Magnet Synchronous Motors," J. Magnetism and Magnetic Materials, pp. 600–603, 2002.
- [11] S. Vaez-Zadeh, A.R. Ghasemi, "Design Optimization of Permanent magnet Synchronous Motors for High Torque Capability and Low Magnet Volume," Electric Power Systems Research, Vol.74, pp. 307-313, Mar. 2005.
- [12] J. A. Guemes, A. M. Iraolagoitia, J. I. Del Hoyo and P. Fernandez, "Torque Analysis in Permanent-Magnet Synchronous Motors", IEEE. Trans. on Conversion, vol. 26, no. 1, Mar 2011.
- [13] M. S. Widyana, " Design, Optimization, Construction & Test of Rare-Earth PM Electrical Machines with New Topology for Wind Energy Applications ", P.h.D dissertation, Dept. Elect & comp. Eng, Berlin Univ, pp 16-34, 2006.
- [14] Armco steel Corporation, " The metallurgy of iron and silicon-iron for soft magnetic applications ", technical report, 2011.
- [15] J.F.Gieras, " Permanent Magnet Technology, Design and Application ", Marcel Dekker Inc, London,United Kingdom, 2002.
- [16] Honda, Y. Higaki, T. Morimoto, S. Takeda, " Rotor design optimization of a multi-layer interior permanent-magnet synchronous motor ", IEE Proc -Electric Power Applications, V. 145, Issue: 2, pp. 119-124, 1998.
- [17] A. Yamada, H. Kawano, I. Miki, M. Nakamura, " A Method of Reducing Torque Ripple in Interior Permanent Magnet Synchronous Motor ", Power Conversion Conference, pp, 322 - 325, Nagoya, 2007.
- [18] D. K. Woo, S. Y. Lee, J. H. Seo, H. K. Jung, " Optimal rotor structure design of interior-permanent magnet synchronous machine base on improved niching genetic algorithm ", 18th International Conference on Electrical Machines, IECM 2008.

**Authors:** Javad Soleimani\* and Abolfazl Vahedi\*\*

\*Young Researchers Club, Hamedan Branch, Islamic Azad University, Hamedan, Iran, *corresponding author*.

E-mail: [jsoleimani@iauh.ac.ir](mailto:jsoleimani@iauh.ac.ir) or [jsoleimani@iee.org](mailto:jsoleimani@iee.org).

\*\*Department Of Electrical Engineering, Iran University of Science & Technology (IUST), Tehran, Iran, E-mail: [avahedi@iust.ac.ir](mailto:avahedi@iust.ac.ir)